BNL-114858-2017-JAAM

Stabilizing CuPd Nanoparticles via CuPd Coupling to WO2.72 Nano-rods in Electrochemical Oxidation of Formic Acid

Z. Xi, D. Su

To be published in "JACS"

October 2017

Center for Functional Nanomaterials

Brookhaven National Laboratory

U.S. Department of Energy

USDOE Office of Science (SC),

USDOE Office of Science (SC), Basic Energy Sciences (BES) (SC-22)

DISCLAIMER

BNL-114858-2017-JA

Stabilizing CuPd Nanoparticles via CuPd Coupling to $WO_{2.72}$ Nanorods in Electrochemical Oxidation of Formic Acid

Z. Xi, D, Su

Accepted by the J. Am. Chem. Soc.

October 2017

Center for Functional Nanomaterials

Brookhaven National Laboratory

U.S. Department of Energy
USDOE Office of Science (SC),
Basic Energy Sciences (BES) (SC-22)

DISCLAIMER

Stabilizing CuPd Nanoparticles via CuPd Coupling to $WO_{2.72}$ Nanorods in Electrochemical Oxidation of Formic Acid

Zheng Xi,[†] Junrui Li,[†] Dong Su,[‡] Michelle Muzzio,[†] Chao Yu,[†] Qing Li[§] and Shouheng Sun[*, †]

†Department of Chemistry, Brown University, Providence, Rhode Island 02912, United States

‡Center for Functional Nanomaterials, Brookhaven National Laboratory, Uptown, New York 11973, United States

§School of Materials Science and Engineering, Huazhong University of Science and Technology, Wuhan, Hubei 430074, China

ABSTRACT: Stabilizing a 3d-transition metal component M from an MPd alloy structure in an acidic environment is key to the enhancement of MPd catalysis for various reactions. Here we demonstrate a strategy to stabilize Cu in 5 nm CuPd nanoparticles (NPs) by coupling the CuPd NPs with perovskite-type $WO_{2.72}$ nanorods (NRs). The CuPd NPs are prepared by controlled diffusion of Cu into Pd NPs and the coupled CuPd/$WO_{2.72}$ are synthesized by growing $WO_{2.72}$ NRs in the presence of CuPd NPs. The CuPd/$WO_{2.72}$ can stabilize Cu in 0.1 M $HClO_4$ solution and, as a result, they show Cu, Pd composition dependent activity for the electrochemical oxidation of formic acid in 0.1 M $HClO_4$ + 0.1 M HCOOH. Among three different CuPd/$WO_{2.72}$ studied, the $Cu_{48}Pd_{52}/WO_{2.72}$ is the most efficient catalyst with its mass activity reaching 2086 mA/mg_{Pd} in a broad potential range of 0.40 to 0.80 V (vs. RHE) and staying at this value after the 12 h chronoamperometry test at 0.40 V. The synthesis can be extended to obtain other MPd/$WO_{2.72}$ (M = Fe, Co, Ni), making it possible to study MPd-$WO_{2.72}$ interactions and MPd stabilization on enhancing MPd catalysis for various chemical reactions.

INTRODUCTION

Developing a robust catalyst for electrochemical formic acid oxidation reaction (FAOR) is an essential step for fabrication of commercially viable direct formic acid fuel cells (DFAFCs).[1-3] Recent efforts taken on searching for advanced FAOR catalysts have helped to better understand the catalytic nature, which in turn, lead to more rational design and tuning of new forms of the catalysts.[4-9] For example, catalysts based on nanostructured Pd have been developed as a potential alternative to Pt for FAOR with better CO tolerance due to their preferential catalysis toward direct 2-electron oxidation of the adsorbed HCOOH* to CO_2, commonly known as dehydrogenation pathway.[10-13] In contrast, the adsorbed HCOOH* on Pt often follows not only the dehydrogenation, but also the dehydration pathway (to CO* + H_2O), causing the undesired Pt surface deactivation by the strong Pt-CO binding.[14] The Pd catalysis can be further improved if a more oxophilic metal (M) is present adjacent to Pd. This M promotes the formation of HO*, which oxidizes CO* on Pd, further increasing the CO tolerance of Pd.[15-16] Despite these advantages demonstrated by Pd over Pt, Pd is chemically less stable than Pt and M in the alloy form is even more prone to fast oxidation and dissolution under the acidic FAOR condition.

A common strategy explored to improve Pd-catalysis is to couple the catalyst with a metal oxide through the strong metal-support interaction to tune Pd electronic/geometric structures and synergistic effects of the oxide support for the desired catalysis,[17] as demonstrated in Pd coupling with CeO_2[18], TiO_2[19], SnO_x[20], HoO_x[21], and MoO_x.[22] We also found that Pd nanoparticles (NPs) coupled with oxygen-deficient perovskite-type $WO_{2.72}$ nanorods (NRs) showed much improved catalytic activity and stability towards the FAOR.[10] Taking advantage of the excellent acid resistance and good electron conductivity of $WO_{2.72}$,[23] here we report that Cu in CuPd alloy NPs can be better stabilized by strong interfacial interactions between the CuPd NPs and $WO_{2.72}$ NRs, as illustrated in **Figure 1**, and the stabilized CuPd shows much improved catalytic ability for the FAOR. Among three different CuPd/$WO_{2.72}$ systems studied, the $Cu_{48}Pd_{52}/WO_{2.72}$ shows the best FAOR performance with its mass activity reaching 2086 mA/mg_{Pd} in a broad potential range of 0.40 to 0.80 V (vs. RHE) in 0.1 M HCOOH + 0.1 M $HClO_4$ and its composition stabilized at $Cu_{40}Pd_{60}/WO_{2.72}$ during the 48 h acid etching test. Our work demonstrates a new strategy to stabilize a 3d-transition metal M from an MPd alloy structure in acid, which will help to develop robust MPd NP catalysts for various chemical reactions.

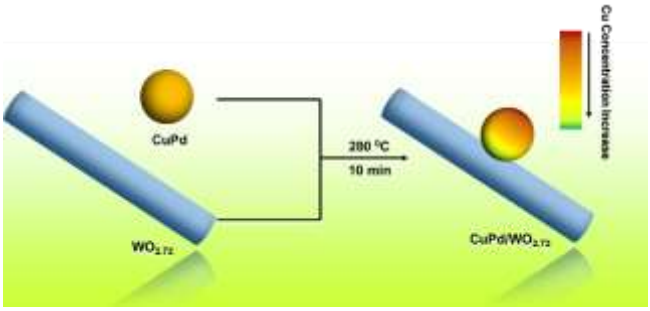

Figure 1. Schematic illustration of the synthesis of CuPd/$WO_{2.72}$ with a CuPd NP coupled to a $WO_{2.72}$ NR, causing Cu to be enriched at the CuPd-$WO_{2.72}$ interface.

EXPERIMENTAL SECTION

Chemicals and Materials. Tungsten (IV) chloride (WCl_4, 97%) and palladium (II) acetylacetonate ($Pd(acac)_2$, 99%) were purchased from Strem Chemicals. Copper (II) acetylacetonate ($Cu(acac)_2$, 97%), borane *tert*-butylamine complex (BBA, 97%), oleylamine (OAm, >70%), oleic acid (OAc, 90%), 1-octadecene

(ODE, 90%) and Nafion solution (5% in a mixture of lower aliphatic alcohols and water) were from Sigma-Aldrich. Hexane (98.5%), ethanol (99%), 2-proponal (99%), perchloric acid (70%) and formic acid (88%) were from Fisher Scientific. These chemicals were used without further purification. The deionized water was obtained from a Millipore Autopure System.

Synthesis of 5 nm Pd NPs. These NPs were prepared according to the method published previously.[10]

Synthesis of 5 nm CuPd NPs. In a typical synthesis, 64 mg (0.25 mmol) $Cu(acac)_2$, 15 mL OAm and 0.32 mL OAc were first mixed by magnetic stirring in a 50 mL four-neck flask and degassed under a gentle flow of N_2 at 70 ^oC for 30 min to form a clear solution. Then 26 mg (0.25 mmol) Pd NPs dispersed in 2 mL hexane was dropped into the solution. The solution was heated to 260 ^oC at 2 ^oC/min and kept at 260 ^oC for 1 h before it was cooled to room temperature. The CuPd NPs were separated by adding 100 mL ethanol and centrifuging at 9500 rpm for 8 min. The product was purified by dispersing in hexane and flocculating with ethanol, and precipitated by centrifugation (9500 rpm, 8 min). The purification process was repeated once and the final NP ($Cu_{49}Pd_{51}$) product was re-dispersed into hexane for further use.

In the same reaction condition, 128 mg (0.50 mmol) $Cu(acac)_2$ and 26 mg (0.25 mmol) Pd NPs gave $Cu_{64}Pd_{36}$ NPs, while 32 mg (0.125 mmol) $Cu(acac)_2$ and 26 mg (0.25 mmol) Pd NPs yielded $Cu_{35}Pd_{65}$ NPs.

Synthesis of CuPd/$WO_{2.72}$. In a typical synthesis, 90 mg (0.27 mmol) WCl_4, 15 mL ODE, 3 mL OAm and 6 mL OAc were first mixed by magnetic stirring in a 50 mL four-neck flask and degassed under a gentle flow of Ar at 120 ^oC for 30 min to form a clear solution. The solution was heated to 280 ^oC in 30 min and kept at 280 ^oC for 10 h, after which, 42 mg (0.25 mmol) $Cu_{49}Pd_{51}$ NPs dispersed in 2 mL ODE was quickly injected into the solution. The solution was kept at 280 ^oC for another 10 min before it was cooled to room temperature. The product, the coupled $Cu_{48}Pd_{52}/WO_{2.72,}$ was separated and purified the same way as described in the synthesis of 5 nm CuPd NPs, and re-dispersed in 20 mL hexane in the presence of one drop of OAm (to better stabilize the composite dispersion) for further use.

In the same reaction condition, mixing 59 mg (0.25 mmol) $Cu_{64}Pd_{36}$ NPs or 35 mg (0.25 mmol) $Cu_{35}Pd_{65}$ NPs with 90 mg (0.27 mmol) WCl_4 yielded $Cu_{63}Pd_{37}/WO_{2.72}$ or $Cu_{33}Pd_{67}/WO_{2.72}$ respectively. Without the addition of CuPd NPs, $WO_{2.72}$ NRs were synthesized as reported previously.[10]

Catalyst Preparation. 20 mg of KetjenBlack EC-300-J carbon (C) was first mixed with 20 mL of hexane and then sonicated for 30 min to form a uniform suspension. Then each of 20 mg CuPd/$WO_{2.72}$, CuPd, and (CuPd + $WO_{2.72}$) physical mixture in hexane was added into the suspension drop-wise under sonication. After 1 h sonication, the C-supported powder was separated by centrifugation (8000 rpm, 8 min), washed with ethanol (3 times) and dried at room temperature. To make the catalysis ink, the C-supported catalyst was mixed with deionized water, 2-propanol and Nafion (V/V/V=4/1/0.05) and sonicated to form a catalyst ink (2 mg/mL). For each test, 20 μL of the catalyst ink was deposited on a newly polished glassy carbon rotating disk electrode (GC-RDE) (0.196 cm^2) and dried in ambient conditions. For each sample, the catalyst (CuPd/$WO_{2.72}$, CuPd or CuPd + $WO_{2.72}$) total mass loading was kept at 0.1 mg/cm^2.

Characterizations. Transmission electron microscopy (TEM) images were acquired from a Philips CM20 (200 kV). High-resolution TEM (HR-TEM) images were obtained from a JEOL 2010 (200 kV). X-ray diffraction (XRD) patterns were collected on a Bruker AXS D8-Advanced diffractometer (Cu Kα λ=1.5418 Å). The inductively coupled plasma-atomic emission spectroscopy (ICP-AES) was measured by a JY2000 Ultrace ICP atomic emission spectrometer equipped with a JYAS 421 autosampler and 2400 g/mm holographic grating. X-ray photoelectron spectroscopy (XPS) was performed on an ESCA 210 and MICROLAB 310D spectrometer using an Mg KR source. Scanning transmission electron microscopy (STEM) analyses were carried out on a Hitachi HD2700C (200 kV) with a probe aberration corrector. The electron energy loss spectroscopy (EELS) line-scan was obtained by a high-resolution Gatan-Enfina ER with a probe size of 1.3 Å.

Electrochemical Measurements. Electrochemical measurements were carried out on an Autolab 302 potentiostat (Eco Chemie B.V, Holland) with GC-RDE (0.196 cm^2) as a working electrode, Ag/AgCl (4 M KCl) as a reference electrode, and graphite rod as a counter electrode. The reference electrode was calibrated to reversible hydrogen electrode (RHE) before the measurements and all potentials were converted to the RHE scale ($V_{Ag/AgCl}$ + 0.26 V = V_{RHE}). The loaded C-catalyst was first subject to potential cycling from 0 to 1.20 V in 50 mL N_2-saturated 0.1 M $HClO_4$ with a scan rate of 100 mV/s to activate the catalytic surface until a stable CV shape was formed (approximately 30 cycles). Then the CV was obtained from 0 to 1.20 V in the N_2-saturated 0.1 M $HClO_4$ with a scan rate of 50 mV/s. The CVs for FAOR were obtained in the N_2-saturated 0.1 M $HClO_4$ + 0.1 M HCOOH electrolyte with a scan rate of 50 mV/s. Chronoamperometry was carried out at the constant potential of 0.40 V in 0.1 M $HClO_4$ + 0.1 M HCOOH with the electrode rotation speed at 1000 rpm. In the CO striping test, the catalyst was first immersed in the CO-saturated 0.1 M $HClO_4$ at 0.10 V for 20 min to form a CO adsorption layer on catalyst surface. Then N_2 was purged into solution for 20 min to remove the remaining CO in solution. CO striping CV was performed from 0 - 1.20 V with a scan rate of 20 mV/s.

RESULTS AND DISCUSSION

Material Synthesis and Characterizations. We first synthesized 5 nm CuPd NPs through seed-diffusion method by using 5 nm Pd NPs as seeds. CuPd NPs were previously prepared either by co-reduction Cu-/Pd-salt precursors with trioctylphosphine (TOP),[15, 24] or oleylamine (OAm) as a surfactant.[16] However, the presence of TOP led to the formation of strong Pd-P bond on the surface of ~ 8 nm NPs and made it difficult to activate these NPs without affecting NP morphology[25] for next step coupling with $WO_{2.72}$. The CuPd NPs prepared in the presence of OAm yielded ~3 nm CuPd NPs, but the method was not readily extended to prepare other MPd NPs with well-controlled sizes and compositions. In the current seed-diffusion synthesis, we used OAm as a solvent, a surfactant and a mild reducing agent, and oleic acid (OAc) as a co-surfactant, and could control the CuPd NP size at ~5 nm at different compositions that were measured by inductively coupled plasma atomic emission spectroscopy (ICP-AES). From the transmission electron microscopy (TEM) image of the as-synthesized $Cu_{49}Pd_{51}$ NPs (**Figure 2A**) and their size analysis (**Figure S1**), we can see that the NPs have an average diameter of 5.3 ± 0.5 nm. The high-resolution TEM (HRTEM) (**Figure 2A inset**) confirms that the CuPd NP has the solid solution structure, not the core/shell structure. The lattice fringe shown in the image has an average spacing of 0.20 nm, which is very close to the (111) interplanar distance of the face-centered cubic (*fcc*) CuPd (111).[26]

To prepare CuPd/$WO_{2.72}$ without NP aggregation, CuPd NPs ($Cu_{49}Pd_{51}$ NPs, for example) were quickly injected into the reac-

tion solution that was used to prepare 50×5 nm $WO_{2.72}$ NRs (**Figure S2**).[27] The reaction progress was monitored by TEM images of the sample products formed at different reaction times (**Figure S3**) and the ideal product ($Cu_{48}Pd_{52}/WO_{2.72}$, for example)) was separated from the reaction solution 10 min after the injection (**Figure 2B & S4**). The HRTEM of a single $Cu_{48}Pd_{52}/WO_{2.72}$ (**Figure 2B inset**) shows the lattice fringe spacing of CuPd (111) at 0.22 nm and $WO_{2.72}$ (010) at 0.38 nm. Comparing with the uncoupled CuPd NPs, we can see that the CuPd NPs in the $CuPd/WO_{2.72}$ structure have their (111) lattice expanded from 0.20 nm to 0.22 nm, which is a good indication of strong coupling between CuPd and $WO_{2.72}$, similar to what was observed in the $Pd/WO_{2.72}$ structure.[10] The reaction condition we used to couple CuPd to $WO_{2.72}$ did not lead to the obvious CuPd composition change – starting from $Cu_{64}Pd_{36}$, $Cu_{49}Pd_{51}$, or $Cu_{35}Pd_{65}$ NPs, we obtained $Cu_{63}Pd_{37}/WO_{2.72}$ $Cu_{48}Pd_{52}/WO_{2.72}$, or $Cu_{33}Pd_{67}/WO_{2.72}$ respectively.

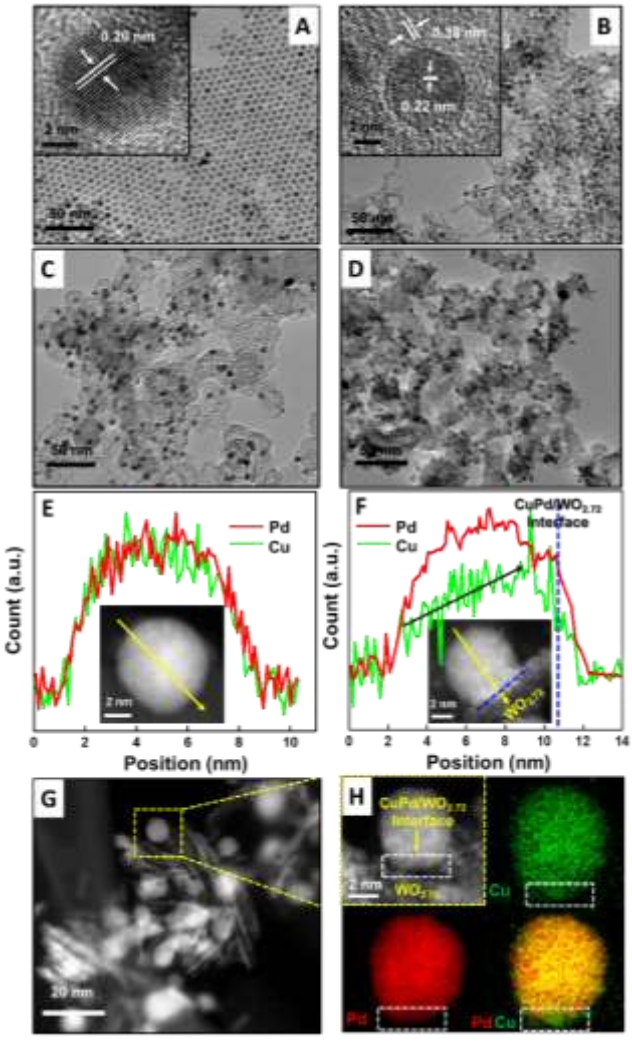

Figure 2. (**A**) TEM image of the as-synthesized 5 nm $Cu_{49}Pd_{51}$ NPs. Inset: HRTEM of a single $Cu_{49}Pd_{51}$ NP. (**B**) TEM image of the as-synthesized $Cu_{48}Pd_{52}/WO_{2.72}$. Inset: HRTEM of one $Cu_{48}Pd_{52}/WO_{2.72}$. (**C, D**) TEM images of the C-$Cu_{49}Pd_{51}$ (**C**) and C-$Cu_{48}Pd_{51}/WO_{2.72}$ (**D**). (**E, F**) STEM-EELS line scan of a single $Cu_{49}Pd_{51}$ NP (**E**) and a $Cu_{48}Pd_{52}$ NP coupled with $WO_{2.72}$ (**F**). (**G**) HAADF-STEM image of C-$Cu_{48}Pd_{52}/WO_{2.72}$ and (**H**) STEM-EELS elemental mapping of a coupled $Cu_{48}Pd_{52}/WO_{2.72}$.

The CuPd and $CuPd/WO_{2.72}$ were deposited on the carbon (C) support, giving C-CuPd and C-$CuPd/WO_{2.72}$, as shown in **Figure 2C&2D**. Both CuPd and $CuPd/WO_{2.72}$ are well-dispersed on C surface. The C-CuPd and C-$CuPd/WO_{2.72}$ were further characterized by atomically resolved aberration-corrected high-angle annular dark-field scanning transmission electron microscopy (HAADF-STEM) and STEM-electron energy loss spectroscopy (STEM-EELS), as shown in **Figure 2E,2F&S5**. The uncoupled CuPd NP shows the uniform alloy composition across the whole NP (**Figure 2E**). As the comparison, the EELS line scan of the CuPd in $CuPd/WO_{2.72}$ reveals a Cu-concentration gradient composition distribution (**Figure 2F&S5**) within the NP. The Cu enrichment at the CuPd-$WO_{2.72}$ interface is also evident in the HAADF-STEM image and the related elemental mapping of the coupled $CuPd/WO_{2.72}$ (**Figure 2G&2H**). From these image, line scan and mapping analyses, we see no clear evidence of Cu deep diffusion into the $WO_{2.72}$ structure, which is different from what we observed in the intercalated $M_xWO_{2.72}$ structure.[28] Our analyses indicate that Cu is attracted more strongly than Pd by $WO_{2.72}$, causing the Cu gradient distribution within the CuPd alloy structure and Cu enrichment at the CuPd-$WO_{2.72}$ interface.

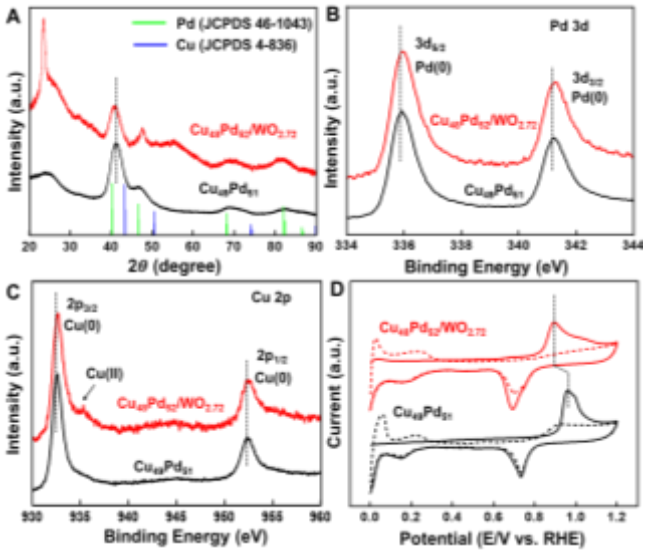

Figure 3. (A) XRD patterns of the C-$Cu_{49}Pd_{51}$ and C-$Cu_{48}Pd_{52}/WO_{2.72}$ with standard peaks of Pd (JCPDS 46-1043) and Cu (JCPDS 4-836). **(B)** Pd 3d XPS spectra of the C-$Cu_{49}Pd_{51}$ and C-$Cu_{48}Pd_{52}/WO_{2.72}$. **(C)** Cu 2p XPS spectra of the C-$Cu_{49}Pd_{51}$ and C-$Cu_{48}Pd_{52}/WO_{2.72}$. **(D)** CO stripping voltammetry of the C-$Cu_{49}Pd_{51}$ and C-$Cu_{48}Pd_{52}/WO_{2.72}$ obtained in 0.1 M $HClO_4$ with a scan rate of 20 mV/s. The solid line is from the first scanning cycle and the dashed line is from the second scanning cycle.

X-ray diffraction (XRD) patterns of both C-CuPd and C-$CuPd/WO_{2.72}$ show that CuPd (111) and (200) peaks locate between the corresponding Pd and Cu peaks, as shown in **Figure 3A**, confirming that the CuPd NPs have the *fcc*-type solid solution structure (We see no evidence of the formation of the B2-CuPd.).[26] The difference between the two samples is that once coupled with $WO_{2.72}$ (there is a characteristic $WO_{2.72}$ (010) peak at 23.5°), the CuPd peaks shift to smaller diffraction angles, indicating the slight lattice expansion of CuPd, which is consistent with the TEM analysis. These two samples were also characterized by X-ray photoelectron spectroscopy (XPS, **Figure S6**). From the Pd 3d spectrum (**Figure 3B**), we can see that both uncoupled CuPd NP and coupled $CuPd/WO_{2.72}$ show a single Pd 3d doublet that can be assigned to $3d_{5/2}$ and $3d_{3/2}$ peaks of Pd (0), which confirms the metallic nature of Pd in both CuPd and $CuPd/WO_{2.72}$.[10] How-

ever, when comparing the detailed peak positions of two samples, we see a slight positive binding energy shift in CuPd/$WO_{2.72}$ than in CuPd ($3d_{5/2}$: 335.94 eV for CuPd/$WO_{2.72}$ and 335.90 eV for CuPd; $3d_{3/2}$: 341.27 eV for CuPd/$WO_{2.72}$ and 341.19 eV for CuPd), which seems to infer a slight decrease of electron density on Pd in the CuPd/$WO_{2.72}$ structure.[29] In the Cu 2p spectrum (**Figure 3C**), we see similar Cu 2p doublets and peak shifts ($2p_{3/2}$: 932.72 eV for CuPd/$WO_{2.72}$ and 932.45 eV for CuPd; $2p_{1/2}$: 952.50 eV for CuPd/$WO_{2.72}$ and 952.40 eV for CuPd), suggesting the metallic character of Cu and the decrease of electron density on Cu. However, the Cu 2p XPS does show an extra, albeit weak, peak at 935.27 eV, which can be assigned to Cu (II).[30] The presence of this Cu (II) feature further supports the observation made from EELS line scan analysis that Cu interacts with $WO_{2.72}$ more strongly than Pd. From the O 1s XPS (**Figure S7**), we see that the peak related to lattice O around 531 eV is negatively shifted once CuPd is coupled with $WO_{2.72}$, while those associated with the adsorbed O (~532.5 eV) and water molecules (534.1eV), which are often observed on a metal oxide surface,[29] stay at the same positions. Similarly, once CuPd coupled with $WO_{2.72}$, the W 4f peak (**Figure S8**) is also negatively shifted. These indicate that in the CuPd/$WO_{2.72}$ structure, there exists a charge transfer from CuPd to $WO_{2.72}$ due to the strong CuPd-$WO_{2.72}$. The slight reduction of surface electron density on CuPd in the CuPd/$WO_{2.72}$ should help to stabilize CuPd and to increase its CO tolerance,[31] which is further confirmed by the CO-stripping tests, as demonstrated in **Figure 3D**. From this test, we see clearly the negative shift of the CO oxidation peak on the CuPd/$WO_{2.72}$ (0.89 V on CuPd/$WO_{2.72}$ vs 0.97 V on CuPd). We expect that the CuPd/$WO_{2.72}$ should promote the FAOR even more towards the dehydrogenation pathway.

Electrocatalysis for FAOR. The FAOR catalysis of the NP samples was studied in 0.1 M $HClO_4$ and 0.1 M HCOOH. Cyclic voltammograms (CVs) of both C-$Cu_{49}Pd_{51}$ NPs and C-$Cu_{48}Pd_{52}/WO_{2.72}$ were first obtained in 0.1 M $HClO_4$, as shown in **Figure S9&4A**. The first CV scan clearly shows the surface Cu oxidation and reduction peaks at around 0.69 V and 0.48 V, respectively. After 30 cycles of CV scans, the NP surface is better conditioned and Cu-oxidation peaks are barely visible.[32] The broader capacitive region and higher proton reduction/hydrogen desorption peaks from the CuPd/$WO_{2.72}$ infer that the catalyst is conductive and has larger electrochemically accessible area. Compared to the metal oxidation peaks that are barely seen in the CVs, the corresponding reduction peaks are easily visible and the peak from the CuPd/$WO_{2.72}$ (0.68 V) is negatively shifted from that of the CuPd (0.71 V), indicating that there is more Cu present in the CuPd/$WO_{2.72}$ than in the CuPd.[32, 33] When 0.1 M HCOOH is present in the 0.1 M $HClO_4$, the CVs of both samples show the typical FAOR catalysis behaviors (**Figure 4B**). From the forward anodic scan in the presence of C-CuPd, we can see a FA oxidation peak around 0.60 V after which the current density starts to drop. The weak oxidation peak at 0.84 V corresponds to CO oxidation, which is typical for the Pd-catalyzed FAOR.[9] This indicates that dehydration pathway still exists on the surface of the CuPd. Similar scanning in the presence of CuPd/$WO_{2.72}$ gives a quite different CV behavior from the CuPd. The current density in the anodic scan reaches sharply to near maximum value at around 0.40 V and stays (with monotonic increase to over 2000 mA/mg_{Pd}) at this high value till the scanning potential reaches 0.80 V, after which Pd is oxidized and the FAOR current drops sharply. From this CV behavior, we cannot see the peak related to CO-oxidation as observed in the CuPd case. The fast increase in the FAOR current density and the lack of CO-oxidation peak indicate that the FAOR is catalyzed by CuPd/$WO_{2.72}$ predominantly via the dehydrogenation pathway.

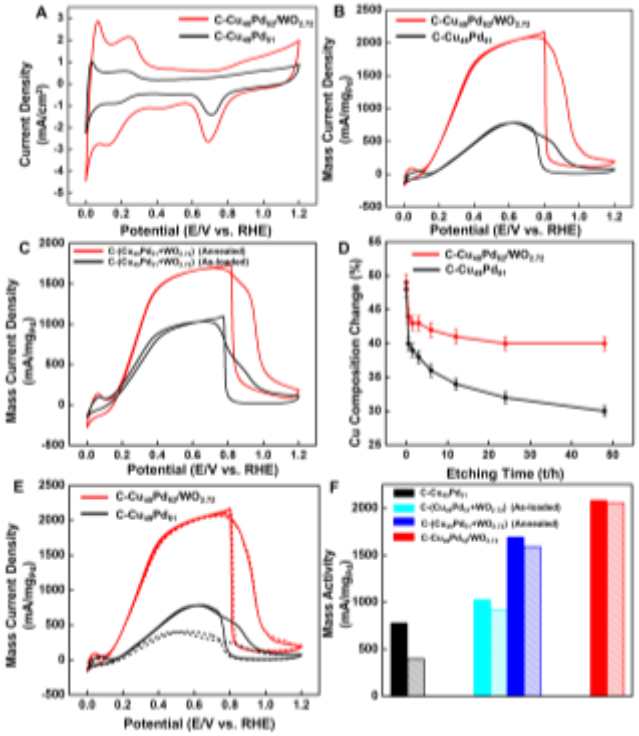

Figure 4. **(A)** CVs and **(B)** FAOR CVs for the C-$Cu_{49}Pd_{51}$ and C-$Cu_{48}Pd_{52}/WO_{2.72}$. **(C)** FAOR CVs for the physical mixture of C-($Cu_{49}Pd_{51}$+$WO_{2.72}$) as-loaded and annealed. **(D)** Cu composition change during the acid etching test in 0.1 M HCOOH + 0.1 M $HClO_4$ solution. **(E)** CVs for the C-$Cu_{49}Pd_{51}$ and C-$Cu_{48}Pd_{52}/WO_{2.72}$ before (solid line) and after (dashed line) 12 h chronoamperometry test at 0.40 V (**F**) FAOR mass activity for C-$Cu_{49}Pd_{51}$, C-$Cu_{48}Pd_{52}/WO_{2.72}$ and C-($Cu_{49}Pd_{51}$+$WO_{2.72}$). Solid bars are before stability test and dashed bars are after stability test. The CVs were obtained at a scan rate of 50 mV/s.

To prove that the strong coupling between CuPd and $WO_{2.72}$ is key to the observation of the enhanced catalysis, we performed a control experiment by physically mixing $Cu_{49}Pd_{51}$ NPs and $WO_{2.72}$ NRs through sonication (mixture molar ratio 1:1, **Figure S10**) and by depositing the physical mixture onto the C-support at room temperature (**Figure S11**). The C-(CuPd+$WO_{2.72}$) was further annealed in an Ar atmosphere at 300 ^oC for 1 h (**Figure S11**) to improve the NP and NR interactions. **Figure 4C** summarizes the FAOR activity of this mixture. We can see that the as-prepared mixture functions similarly to the C-CuPd, but the annealed mixture shows degrees of improvement in its catalysis with its CV behavior getting close to that of the C-CuPd/$WO_{2.72}$ (still less active than the C-CuPd/$WO_{2.72}$ due to the less degree of the control of the CuPd-$WO_{2.72}$ interactions in the physical mixture). Combining what we observed from the C-CuPd, C-CuPd/$WO_{2.72}$ and C-(CuPd+$WO_{2.72}$) catalyzed FAOR, we can conclude that strong coupling between CuPd and $WO_{2.72}$ is indeed necessary for CuPd NPs to show the enhanced catalysis for the FAOR.

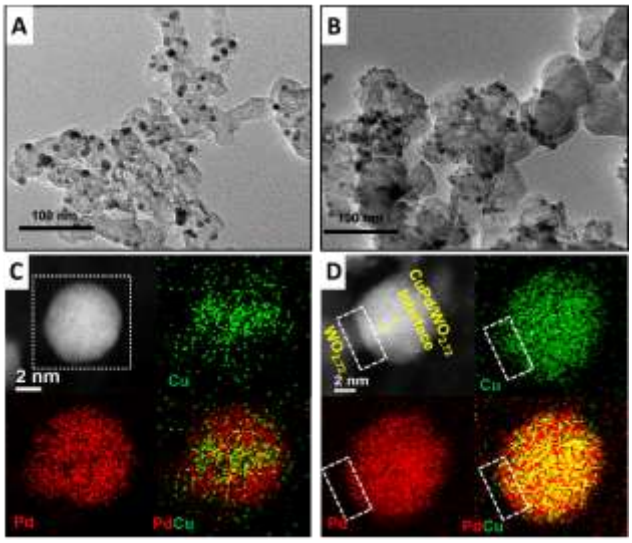

Figure 5. TEM images of (**A**) C-$Cu_{49}Pd_{51}$ and (**B**) C-$Cu_{48}Pd_{52}/WO_{2.72}$, as well as STEM-EELS elemental mapping of a representative (**C**) $Cu_{49}Pd_{51}$, and (**D**) $Cu_{48}Pd_{52}/WO_{2.72}$ after 12 h chronoamperometry test at 0.40 V.

The strong coupling between CuPd and $WO_{2.72}$ helps to stabilize Cu against fast acid etching and to enhance CuPd catalysis for the FAOR. **Figure 4D** shows the Cu-concentration change of both C-$Cu_{49}Pd_{51}$ and C-$Cu_{48}Pd_{52}/WO_{2.72}$ during the 48 h acid etching test in 0.1 M HCOOH + 0.1 M $HClO_4$. Aliquots were taken at each time point and ICP-AES was applied to monitor the Cu composition changes. The test shows that the C-CuPd/$WO_{2.72}$ retains a large amount of Cu and the Cu, Pd composition is stabilized at $Cu_{40}Pd_{60}$. As a comparison, the C-CuPd has poor Cu-retaining ability with Cu being etched away slowly in the 48 h etching test. The enhanced stability of C-CuPd/$WO_{2.72}$ over C-CuPd is further shown in the steady FAOR behavior demonstrated by C-CuPd/$WO_{2.72}$ after the 12 h chronoamperometry test at 0.40 V (**Figure 4E**) in which the curve from the C-CuPd/$WO_{2.72}$ is nearly unchanged while that from the C-CuPd exhibits the obvious drop, which is consistent with the Pd-catalyzed FAOR.[34, 35] The mass activity of the C-CuPd/$WO_{2.72}$ can be stabilized around 2086 mA/mg_{Pd} after 12 h chronoamperometry test at 0.40V, while that of the C-CuPd drops from 779 to 398 mA/mg_{Pd} (**Figure 4F**). Analyzing the C-CuPd and C-CuPd/$WO_{2.72}$ after the 12 h chronoamperometry test using TEM and STEM-EELS mapping (**Figure 5**), we can see that CuPd NPs in both C-CuPd and C-CuPd/$WO_{2.72}$ show no obvious morphology changes (**Figure 5A, B**), but the alloy structure is much better stabilized in the C-CuPd/$WO_{2.72}$ than in the C-CuPd (**Figure 5C, D**). There is an obvious Cu loss from the C-CuPd and the alloy CuPd NPs are turned into core/shell CuPd/Pd NPs (**Figure 5C**). As a comparison, the CuPd NPs in the C-CuPd/$WO_{2.72}$ have predominantly an alloy-type structure with a slight Pd-enrichment on the NP surface (**Figure 5D&S12**). The stability of C-(CuPd+$WO_{2.72}$), both as-loaded and annealed, is between that of C-CuPd and C-CuPd/$WO_{2.72}$ (**Figure 4F&S13**).

$WO_{2.72}$ NRs are also effective in stabilizing other CuPd NPs. $Cu_{64}Pd_{36}$ NPs (5.6 ± 0.6 nm) and $Cu_{35}Pd_{65}$ NPs (5.1 ± 0.5 nm) (**Figure S14**) were prepared and coupled to $WO_{2.72}$ NRs, giving $Cu_{63}Pd_{37}/WO_{2.72}$ and $Cu_{33}Pd_{67}/WO_{2.72}$ (**Figure S15**) respectively. The NPs show typical XRD pattern of the CuPd NPs with slight changes in diffraction angles (**Figure S16&3A**). Their acid stability was tested in 0.1 M HCOOH + 0.1 M $HClO_4$ solution for 48 h and the Cu change during this time period was monitored by ICP-AES, as shown in **Figure S17**. We can see clearly the effect of the $WO_{2.72}$ stabilization: the $Cu_{64}Pd_{36}$ NPs are stabilized at $Cu_{41}Pd_{59}$ and $Cu_{33}Pd_{67}$ NPs at $Cu_{25}Pd_{75}$. After 12 h chronoamperometry test at 0.40 V, we observed no obvious NP morphology change on these $WO_{2.72}$ coupled samples (**Figure S18**). As a result, the CuPd/$WO_{2.72}$ NPs show much enhanced catalysis for the FAOR (**Figure S19**).

Our studies show that efficient coupling between CuPd and $WO_{2.72}$ is essential to protect Cu from heavy loss from the CuPd alloy structure in acid and to retain the high catalytic efficiency of CuPd in the FAOR condition. Comparing with all three different kinds of CuPd/$WO_{2.72}$ and CuPd NPs we have tested, we can conclude that 1) the CuPd/$WO_{2.72}$ catalyst is much more active than the CuPd one; 2) the CuPd/$WO_{2.72}$ shows Cu/Pd composition-dependent catalysis; and 3) the $Cu_{48}Pd_{52}/WO_{2.72}$ catalyst is most active and stable for the FAOR. The high activity and stability demonstrated by CuPd/$WO_{2.72}$ makes it a promising class of Pd-catalyst that can replace Pt-catalyst for highly efficient FAOR.

CONCLUSION

In this paper, we demonstrate a new strategy to stabilize CuPd NPs by coupling CuPd NPs with $WO_{2.72}$ NRs. The 5 nm CuPd NPs are prepared by controlled diffusion of Cu into Pd NPs, and $WO_{2.72}$ NRs are grown in the presence of CuPd NPs, forming the CuPd/$WO_{2.72}$ composites. Due to the strong CuPd-$WO_{2.72}$ coupling, the CuPd (111) lattice is expanded and Cu is pulled towards $WO_{2.72}$, causing Cu to enrich at the CuPd-$WO_{2.72}$ interface. The Cu in the CuPd/$WO_{2.72}$ is much better stabilized in 0.1 M $HClO_4$ and the 48 h etching changes the $Cu_{48}Pd_{52}/W_{2.72}$ to a stable form in $Cu_{40}Pd_{60}/WO_{2.72}$. The CuPd/$WO_{2.72}$ is very active and stable in catalyzing the FAOR in 0.1 M $HClO_4$ + 0.1 M HCOOH. Among three different CuPd/$WO_{2.72}$ studied in this paper, the $Cu_{48}Pd_{52}/W_{2.72}$ shows the best catalytic performance with its mass activity reaching 2086 mA/mg_{Pd} in a broad potential range of 0.40 to 0.80 V (vs. RHE) without activity drop in the 12 h chronoamperometry test at 0.40 V. The CuPd/$WO_{2.72}$ is among the most active Pd-based NP catalyst ever reported for the FAOR (**Table S1**) and has the potential to replace Pt to catalyze the FAOR. The reported seed-diffusion method is not limited to the synthesis of CuPd NPs, but can be extended to the preparation of other MPd NPs (M = Fe, Co and Ni) as well (**Figure S20** and **Table S2**), providing a general approach to the production of MPd/$WO_{2.72}$ for studying MPd-$WO_{2.72}$ interactions and their effect on M stabilization and M-enhanced Pd catalysis for various chemical reactions.

ASSOCIATED CONTENT

The Supporting Information contains figures and tables for additional materials characterizations and more electrochemical measurements and is available free of charge via the Internet at http://pubs.acs.org.

AUTHOR INFORMATION

Corresponding Author

* ssun@brown.edu

Notes

The authors declare no competing financial interests.

ACKNOWLEDGMENT

The work was supported by the U.S. Army Research Laboratory and the U.S. Army Research Office under grant W911NF-15-1-

0147 and under the Multi University Research Initiative (MURI) W911NF-11-1-0353. Part of electron microscopy work was carried out at the Center for Functional Nanomaterials, Brookhaven National Laboratory (BNL), which is supported by the DOE, Office of Basic Energy Sciences, under contract DE-SC-0012704. Q. L. thanks for financial support from National Nature Science Foundation of China (21603078) and National Materials Genome Project (2016YFB0700600). M. M. is supported by the National Science Foundation Graduate Research Fellowship under Grant 1644760.

REFERENCES

(1) Yu, X. W.; Pickup, P. G. *J. Power Sources* **2008**, *182*, 124−132.
(2) Demirci, U. B. *J. Power Sources* **2007**, *169*, 239−246.
(3) Qian, W. M.; Wilkinson, D. P.; Shen, J.; Wang, H. J.; Zhang, J. J. *J. Power Sources* **2006**, *154*, 202−213.
(4) Ji, X.; Lee, K. T.; Holden, R.; Zhang, L.; Zhang, J.; Botton, G. A.; Couillard, M.; Nazar, L. F. *Nat. Chem.* **2010**, *2*, 286−293.
(5) Zhang, S.; Guo, S.; Zhu, H.; Su, D.; Sun, S. *J. Am. Chem. Soc.* **2012**, *134*, 5060−5063.
(6) Kang, Y.; Qi, L.; Li, M.; Diaz, R. E.; Su, D.; Adzic, R. R.; Stach, E.; Li, J.; Murray, C. B. *ACS Nano* **2012**, *6*, 2818−2825.
(7) Xi, Z.; Lv, H.; Erdosy, D. P.; Su, D.; Li, Q.; Yu, C.; Li, J.; Sun, S. *Nanoscale* **2017**, *9*, 7745-7749.
(8) Neurock, M.; Janik, M.; Wieckowski, A. *Faraday Discuss* **2008**, *140*, 363–378.
(9) Zhang, R. G.; Liu, H. Y.; Wang, B. J.; Ling, L. X. *J. Phys. Chem. C* **2012**, *116*, 22266-22280.
(10) Xi, Z.; Erdosy, D. P.; Mendoza-Garcia, A.; Duchesne, P. N.; Li, J.; Muzzio, M.; Li, Q.; Zhang, P.; Sun, S. *Nano Lett.* **2017**, *17*, 2727-2731.
(11) Huang, X.; Tang, S.; Mu, X.; Dai, Y.; Chen, G.; Zhou, Z.; Ruan, F.; Yang, Z.; Zheng, N. *Nat. Nanotechnol.* **2011**, *6*, 28-32.
(12) Choi, S. I.; Herron, J. A.; Scaranto, J.; Huang, H. W.; Wang, Y.; Xia, X. H.; Lv, T.; Park, J. H.; Peng, H. C.; Mavrikakis, M.; Xia, Y. N. *ChemCatChem* **2015**, *7*, 2077−2084.
(13) Chang, J. F.; Feng, L. G.; Liu, C. P.; Xing, W.; Hu, X. L. *Angew. Chem., Int. Ed.* **2014**, *53*, 122−126.
(14) Jiang, K.; Zhang, H. X.; Zou, S.; Cai, W. B. *Phys. Chem. Chem. Phys.* **2014**, *16*, 20360-20376.
(15) Mazumder, V.; Chi, M.; Mankin, M. N.; Liu, Y.; Metin, O.; Sun, D.; More, K. L.; Sun, S. *Nano Lett.* **2012**, *12*, 1102-1106.
(16) Ho, S. F.; Mendoza-Garcia, A.; Guo, S.; He, K.; Su, D.; Liu, S.; Metin, O.; Sun, S. *Nanoscale* **2014**, *6*, 6970-6973.
(17) Kattel, S.; Liu, P.; Chen, J. G. *J. Am. Chem. Soc.* **2017**, *139*, 9739-9754.
(18) Miller, H. A.; Lavacchi, A.; Vizza, F.; Marelli, M.; Di Benedetto, F.; D'Acapito, F.; Paska, Y.; Page, M.; Dekel, D. R. *Angew. Chem., Int. Ed.* **2016**, *55*, 6004−6007.
(19) Liu, P.; Zhao, Y.; Qin, R.; Mo, S.; Chen, G.; Gu, L.; Chevrier, D. M.; Zhang, P.; Guo, Q.; Zang, D.; Wu, B.; Fu, G.; Zheng, N. *Science* **2016**, *352*, 797-801.
(20) Freakley, S. J.; He, Q.; Harrhy, J. H.; Lu, L.; Crole, D. A.; Morgan, D. J.; Ntainjua, E. N.; Edwards, J. K.; Carley, A. F.; Borisevich, A. Y.; Kiely, C. J.; Hutchings, G. J. *Science* **2016**, *351*, 965−968.
(21) Feng, L.; Sun, X.; Liu, C.; Xing, W. *Chem. Commun*. **2012**, *48*, 419−421.
(22) Lim, E.J.; Kim, H.J.; Kim, W.B.; *Catalysis Communications.* **2012**, *25*, 74-77.
(23) Xi, G.; Ouyang, S.; Li, P.; Ye, J.; Ma, Q.; Su, N.; Bai, H.; Wang, C. *Angew. Chem., Int. Ed*. **2012**, *51*, 2395−2399.
(24) Wang, C.; Chen, D. P.; Sang, X.; Unocic, R. R.; Skrabalak, S. E. *ACS Nano* **2016**, *10*, 6345-6353.
(25) Liu, Y.; Wang, C.; Wei, Y.; Zhu, L.; Li, D.; Jiang, J. S.; Markovic, N. M.; Stamenkovic, V. R.; Sun, S. *Nano Lett.* **2011**, 11, 1614-1617.
(26) Jiang, K.; Wang, P.; Guo, S.; Zhang, X.; Shen, X.; Lu, G.; Su, D.; Huang, X. *Angew. Chem. Int. Ed*. **2016**, *55*, 1-7.
(27) Yu, C.; Guo, X.; Xi, Z.; Muzzio, M.; Yin, Z.; Shen, B.; Li, J.; Seto, C.; Sun, S. *J. Am. Chem. Soc*. **2017**, *139*, 5712-5715.
(28) Xi, Z.; Mendosa-Garcia, A.; Zhu, H.; Chi, M.; Su, D.; Erdosy, P. D.; Li, J.; Sun, S. *Green Energy & Environment* **2017**, *2*, 119-123.
(29) Lu, Y.; Jiang, Y.; Gao, X.; Wang, X.; Chen, W. *J. Am. Chem. Soc.* **2014**, *136*, 11687−11697.
(30) Li, Q.; Fu, J.; Zhu, W.; Chen, Z.; Shen, B.; Wu, L.; Xi, Z.; Wang, T.; Lu, G.; Zhu, J. J.; Sun, S. *J. Am. Chem. Soc*. **2017**, *139*, 4290-4293.
(31) Chen, G.; Xu, C.; Huang, X.; Ye, J.; Gu, L.; Li, G.; Tang, Z.; Wu, B.; Yang, H.; Zhao, Z.; Zhou, Z.; Fu, G.; Zheng, N. *Nat. Mater*. **2016**, *15*, 564-569.
(32) Cui, C. H.; Yu, S. H. *Acc. Chem. Res.* **2013**, *46*, 1427-1437.
(33) Jiang, G.; Zhu, H.; Zhang, X.; Shen, B.; Wu, L.; Zhang, S.; Lu, G.; Wu, Z.; Sun, S.; *ACS Nano* **2015**, *9*, 11014-11022.
(34) Li, H. H.; Fu, Q. Q.; Xu, L.; Ma, S. Y.; Zheng, Y. R.; Liu, X. J.; Yu, S. H. *Energ. Environ. Sci.* **2017**, *10*, 1751-1756.
(35) Ma, S. Y.; Li, H. H.; Hu, B. C.; Cheng, X.; Fu, Q. Q.; Yu, S. H. *J. Am. Chem. Soc.* **2017**. *139*, 5890-5895.

TOC: